CHINESE OPTICS LETTERS

Vol. 19, No. 3 | March 2021

Optoelectronic and elastic properties of metal halides double perovskites Cs_2InBiX_6 (X = F, Cl, Br, I)

Muhammad Saeed[1,2], Izaz Ul Haq[3], Shafiq Ur Rehman[4], Akbar Ali[3], Wajid Ali Shah[3], Zahid Ali[3], Qasim Khan[5**], and Imad Khan[3*]

[1] State Key Laboratory of Nuclear Resources and Environment, East China University of Technology, Nanchang 330013, China

[2] College of Nuclear Science and Engineering, East China University of Technology, Nanchang 330013, China

[3] Center for Computational Materials Science, Department of Physics, University of Malakand, Chakdara, Pakistan

[4] College of Physics and Optoelectronic Engineering, Shenzhen University, Shenzhen 518060, China

[5] College of Electronic Science and Technology, Shenzhen University, Shenzhen 518000, China

*Corresponding author: imadkhan723@gmail.com

**Corresponding author: qasim@szu.edu.cn

Received November 20, 2020 | Accepted January 19, 2021 | Posted Online March 12, 2021

Structural geometry, electronic band gaps, density of states, optical and mechanical properties of double perovskite halides Cs_2InBiX_6 (X = F, Cl, Br, I) are investigated using the density functional theory. These compounds possess genuine perovskite stoichiometry, evaluated using various geometry-based indices like tolerance factor, octahedral factor, and formation energy. The fundamental electronic band gaps are direct and valued in the range 0.80–2.79 eV. These compounds have narrow band gaps (except Cs_2InBiF_6) due to strong orbital coupling of the cations. The valence band maximum and conduction band minimum are confirmed to be essentially of In 5s and Bi 6p characters, respectively. The splitting of Bi 6p bands due to strong spin-orbit coupling causes reduction in the band gaps. These compounds have large dispersion in their bands and very low carrier effective masses. The substitution of halogen atoms has great influence on the optical properties. The mechanical properties reveal that Cs_2InBiX_6 (X = F, Cl, Br, I) satisfy the stability criteria in cubic structures.

Keywords: optical materials; metal halides; density functional theory; perovskite stoichiometry; spin-orbit coupling.

DOI: 10.3788/COL202119.030004

1. Introduction

The appearance of lead (Pb) tri-halide perovskites $APbX_3$ in photovoltaic cells resulted in power conversion efficiency up to 25.2% in 2020[1,2], which offers an extraordinary prospect for wider use of solar energy. Pb halide perovskites have exceptional properties such as high charge carrier mobilites, direct and tunable band gaps, small effective masses of electrons and holes, high absorption, balanced electron and hole transport, and long carrier diffusion length[3–9]. Due to the remarkable structural, electrical, optical, electronic, magnetic, catalytic, and superconducting properties, halide perovskites find many applications in new areas of technology[10–14]. They are widely used as optical functional materials in different devices like light emitting diodes (LEDs), solar cell absorbers, X-ray detectors, lasers, batteries, photodetectors, and quantum dots[15–20]. Extensive research has been carried out on photovoltaic hybrid organic–inorganic perovskites (ABX_3) using Pb as a B-site cation from the last 10 years[21–23]. However, Pb perovskites undergo intrinsic structure instability when exposed to moisture, light, air, and high temperatures. In addition, Pb is a most toxic element and compounds containing high content of Pb are reported harmful to health and the environment[24,25].

Overcoming this toxicity and instability problem gives rise to research work committed to investigating Pb free perovskites free of intrinsic structure instability and poverty under external stimuli[24,26]. It is highly desirable to identify Pb free materials that have properties of the extensively studied $MAPbX_3$ perovskites[3]. The effective replacement of Pb from perovskite halides leads us to adopt different structural designs. Pb can be replaced by other group IV elements, e.g., Ge and Sn, as $CH_3NH_3SnI_3$ and $CH_3NH_3GeI_3$, but their use provides chemical instability due to the preferred poor +4 oxidation state and poor optoelectronic performance[27]. Inorganic perovskites $CsPbX_3$ (X = F, Cl, Br, and I) are more thermally stable in contrast to organic–inorganic hybrid perovskites[28–30]. Alternatively, two Pb can be replaced by a pair of monovalent and trivalent ions leading to the structure of organic/inorganic double perovskites having the general formula $AB^+B^{3+}X_6$ (A = organic or alkaline earth metal, B^+ = monovalent, B^{3+}= trivalent, X = halogen)[18]. The crystal structure of double

perovskite is stable and the same as in most oxides. Moreover, introducing different metal cations on site B, diverse organic and inorganic cations on site A, and a variation of halide compositions on site X can fabricate highly efficient materials comparable to $MAPbI_3$ ($MA = CH_3NH_3$) and $CsPbI_3$[26,31]. Double perovskite halides are emerging efficient materials in numerous applications such as ferroelectrics, electrocatalysts, phosphors, white light emitters, spintronics, magnetoresistive materials, and solar absorbers[32,33]. The early synthesized organic double perovskite methyl ammonium $[CH_3NH_3]^+$ and formamidinium $[NH_2CHNH_2]^+$ are not stable and not suitable for the use of photovoltaic cells[34–38]. Small amounts of inorganic cations like Cs^+ doping with methylammonium $[CH_3NH_3]^+$ and formamidinium $[NH_2CHNH_2]^+$ at the A site can raise the stability of perovskites[29,39–42]. Inorganic double perovskite halides $AB^+B^{3+}X_6$ (with B^{3+} = Sb, Bi; B^+ = Ag, Cu, Au, and X = Cl, Br, I) are useful for optoelectronic purposes when their band gaps lie in the visible range of the electromagnetic spectrum[43]. The successful candidates for solar cells are $Cs_2AgBiCl_6$ and $Cs_2AgBiBr_6$. These compounds are more stable and absorb light in the visible range of the electromagnetic spectrum. The structures of these compounds are highly symmetric faces of center cubic double perovskites. $Cs_2AgBiCl_6$ and $Cs_2AgBiBr_6$ are indirect band gap semiconductors, and $Cs_2AgBiBr_6$ is s synthetically stable and non-harmful perovskite having a band gap of 2.19 eV by diffuse reflectance spectroscopy and 1.95 eV by photoluminescence[44,45]. It has limited applications in photo cells because of its low absorption of light[46].

In metal halides perovskites, the A-site cation is not involved in the formation of the frontier band edges; on the other hand, anions at the X site (F, Cl, Br, I) modulate the size [in electron volts (eV)] of the band gap but have nothing with the orbital character and direct/indirect nature of the band gap[47]. Therefore, the efficiency of metal halide perovskites in solar cells and LEDs can be tuned by smart choices of B^+ and B^{3+} sites cations. Choices for the B^{3+} site are (i) elements of group III (In, Tl), (ii) pnictogens, and (iii) several transition metals (Cr, Mn). For the B^+ site, the possible candidates are (i) noble transition metals (Ag, Au), (ii) lanthanides, (iii) some actinides (Pu, Am, and Bk), (iv) elements of group III (In, Tl), and (v) alkaline metals (Na, K). Among these, lanthanides, actinides, and transition metals have partially f or d orbitals, so they would have band extremes of such states. Group III elements in the +3 oxidation state have the highest occupied states of the d character at the top of the valence band. The pnictogens such as N^{3+} and P^{3+} are not stable in perovskite structures because of their small size, according to Goldschmidt's rule. Arsenic is toxic, and the possible candidates to realize double perovskites from the pnictogen family are Sb^{3+} and Bi^{3+}.

Potential contestants for the B^+ site in double perovskite halides are alkaline metals, elements of group III, and noble transition metals. Out of these three, alkaline metals give non-dispersive bands and hence are not suitable for photovoltaic perspectives. Cations of the noble transition metals occupy the highest orbital of the d character when it is in the +1 oxidation state. This situation will lead to valence band maximum of the d character and is not needed[26]. Group III elements have filled s and d orbitals when they are in the +1 oxidation state; in this configuration, d electrons are deeper than s electrons. The suitable elements from group III are In and Tl (the rest have low atomic numbers and cannot exist in the +1 oxidation state); as Tl is toxic, the sole option for us is In [48].

Zhao *et al.*[49] proposed that In^{1+}-based double perovskites $Cs_2InBiCl_6$ and $Cs_2InSbCl_6$ are useful solar cell absorbers because their band gaps are direct, having band gaps of 1.02 eV and 0.91 eV, respectively. These predictions were provided by the relatively new hybrid functional, including spin-orbit coupling (SOC) [Heyd–Scuseria–Ernzerhof (HSE + SOC)] calculations. These two perovskites are found to be thermodynamically stable against decomposition with small effective masses of electrons and holes[50]. The In^{1+} oxidation state is rare; however, InCl and $In_3Ti_2Br_9$ are the compounds in which the In^{1+} oxidation state has been reported[51,52]. Although theoretical studies proposed that Cs_2InBiX_6 and Cs_2InSbX_6 (X = Cl, Br, I) have admirable optoelectronic properties including direct band gaps and small carrier effective masses, they are unstable due to the favorable +3 oxidation state of In [53]. To the best of our knowledge, successful synthesis of these double perovskites has not been reported. The replacement of the A-site cation in these compounds with a large sized mixed cation such as $(Cs/MA/FA)_2InBiBr_6$ can passivate the oxidation process and might solve the stability problem[26,32,47]. Substitution of the A-site cations can provide stability to double perovskites[29,39–42], but have no contribution in the formation of frontier bands and therefore have negligible effects on the optoelectronic properties[2,47]. These compounds have been studied theoretically, yet there is a lack of literature about their elastic and optoelectronic nature. In this article, an attempt has been made to study the stability and effect of anion substitution on the structural, chemical bonding, electronic, elastic, and optical properties of Cs_2InBiX_6 (X = F, Cl, Br, I) using different exchange-correlation approximations of the density functional theory (DFT). These compounds are direct band materials in contrast to other inorganic double perovskites. The calculated band gap of $Cs_2InBiCl_6$ is 1.37 eV, close to the optimal band gap (1.4 eV) for photovoltaic applications. The absorption edge of these compounds is found to be similar to the best-identified material ($MAPbI_3$) for solar cells. The present work will not only to help us understand the optoelectronic and mechanical properties of Cs_2InBiX_6 (X = F, Cl, Br , I), but will also motivate researchers to explore double perovskite halides for practical applications.

2. Details of Calculations

DFT is used to calculate the structural, electronic, optical, and elastic properties of Pb free inorganic double perovskite halides Cs_2InBiX_6 (X = F, Cl, Br , I). The calculations are done using the full potential linearized augmented plane wave (FP-LAPW) method implemented in the Wein2k package[54].

Exchange-correlation energy is dealt by generalized gradient approximation (GGA) Perdew–Burke–Ernzerhof for solids (PBEsol)[55], because it is more effective compared to other GGA characteristics for the calculation of structure optimization[56]. For the calculations of electronic properties of GGA, modified Becke–Johnson (mBJ) and mBJ with SOC (mBJ + SOC) are used. GGA often gives much underestimated results as compared to experiments[57,58]. The mBJ[59,60] exchange potential in addition to GGA is known for its remarkable success in reproducing experimental band gaps of semiconductors in general and halide perovskites in particular[60]. These compounds contain heavy elements like Bi; therefore, SOC calculations have been carried out for better treatment of different orbital splitting in electronic and optical properties. Self-consistent calculations throughout the Brillouin zone were carried out using 2×10^6 points.

3. Results and Discussion

3.1. Structural Properties

The crystal structure of Cs_2InBiX_6 is cubic and belongs to space group Fm-3m (225)[49]. The unit cell structure of Cs_2InBiX_6 (X = F, Cl, Br, and I) shown in Fig. 1 possesses 10 atoms. The figure illustrates that, like the basic perovskite structure (ABX_3), double perovskite $A_2B^+B^{3+}X_6$ is a three-dimensional (3D) framework, in which the A cation (here Cs^+) occupies the cubic octahedral cavity formed by corner shearing of In and Bi octahedra. These octrahedra have fascinating roles in the physical properties of perovskites.

In order to get ground state energies, unit cells of Cs_2InBiX_6 (X = F, Cl, Br, and I) are optimized using the reported[49] lattice parameters, symmetry of the space group, and atomic coordinates. Total energy versus volume curves are plotted in Fig. 2 for Cs_2InBiX_6 compounds, and the obtained values are then fitted to Birch Murnaghan's equation of states[61]. The calculated lattice constants are listed in Table 1. Halogen replacement

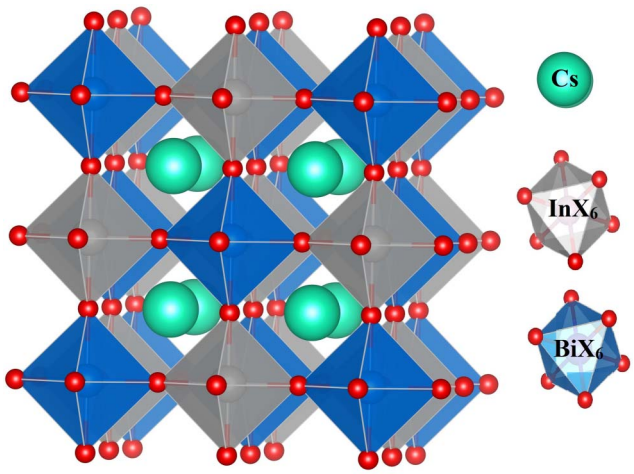

Fig. 1. Unit cell structure of Cs_2InBiX_6 (X = F, Cl, Br, and I).

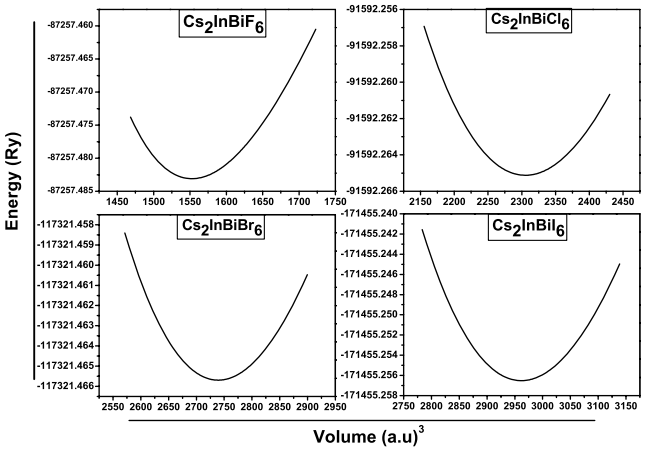

Fig. 2. Energy versus volume optimization curves of Cs_2InBiX_6 (X = F, Cl, Br, I).

Table 1. Calculated Tolerance Factor τ, Octahedral Factor μ, Lattice Constants a, Bond Lengths r_{ij}, Band Gap E_g, and Effective Masses of Electrons m_e^* and Holes m_h^* (m_o) of Cs_2InBiX_6.

Parameters		X = F	X = Cl	X = Br	X = I
a (Å)		9.70	11.07	11.30	12.32
		9.80[a]	11.44[a]	11.93[a]	12.69[a]
τ	Eq. (1)	0.95	0.90	0.89	0.87
	Eq. (3)	3.49	4.01	4.07	4.13
μ		0.68	0.53	0.47	0.44
r_{ij} (Å)	Bi–X (x6)	2.25	2.73	2.79	2.82
	In–X (x6)	2.60	3.00	3.09	3.15
	Cs–X (x12)	3.43	4.06	4.12	4.20
E_g (eV)	GGA	2.01	0.38	0.25	0.12
	mBJ	2.79	1.37	0.82	0.80
	mBJ + SOC	1.87	0.87	0.32	0.23
	HSE + SOC	2.22[a]	1.02[a], 0.88[b]	0[a], 0.33[b]	0[a], 0.21[b]
m_e^*	mBJ	0.73	0.52	0.37	0.28
	mBJ + SOC	0.58	0.38	0.29	0.24
	HSE + SOC	0.61[a]	0.39[a]	0.30[a]	0.23[a]
	$MaPbI_3$				0.19[c]
m_h^*	mBJ	0.46	0.23	0.19	0.13
	mBJ + SOC	0.37	0.19	0.14	0.09
	HSE + SOC	0.39[a]	0.17[a]	0.11[a]	0.08[a]
	$MaPbI_3$				0.25[c]

[a]Reference [31].
[b]Reference [53].
[c]Reference [62].

caused a systematic increase in the lattice constant; this increase is due to the increase in size of anions from F to I.

For structure stability of these double perovskites Cs_2InBiX_6 (X = F, Cl, Br, I), a modified tolerance (τ) factor and an octahedral factor (μ) are calculated from the ionic radii of the different components given in the formulas[63]

$$\tau = \frac{r_A + r_X}{\sqrt{2}(r_B + r_X)}, \tag{1}$$

$$\mu = \frac{r_B}{r_X}, \tag{2}$$

where r_B is the average radius of B^+ and B^{3+}; r_A and r_X are the radii of Cs and halogen atoms. The calculated values of tolerance and octahedral factors are listed and compared with other theoretical results in Table 1. A τ value in the range of $0.8 < \tau < 1.0$ and a μ value in the range of $0.44 < \mu < 0.90$ have been suggested, X atoms in the (100)[49]. The tolerance factor varies between 0.95 and 0.87, and the octahedral factor lies in the range of 0.68 to 0.44; the tolerance and octahedral factors reveal that Cs_2InBiX_6 (X = F, Cl, Br, I) adopts an ideal perovskite structure. The accurate and probabilistic nature of the tolerance factor as well as its applicability over a broad range of perovskites creates a new physical insight into the stability and the prediction of new stable organic, inorganic, and hybrid perovskites. A new tolerance factor formula is used for perovskite structure stability[32]:

$$\tau = \frac{r_X}{r_B} - n_A\left[n_A - \frac{r_A/r_B}{\ln(r_A/r_B)}\right], \tag{3}$$

where n_A is the oxidation state of the A atom. The calculated values of τ using Eq. (3) are listed in Table 1, which clarifies that the values are below 4.18 (stable perovskites are expected when $\tau < 4.18$)[32]. The tolerance and octahedral factors confirm the stability of Cs_2InBiX_6 in cubic crystal structures, and, hence, these compounds are investigated in elpasolite structures with space group Fm-3m, which corresponds to an ideal double perovskite.

Formation energies of Cs_2InBiX_6 (X = F, Cl, Br, I) compounds have been calculated in order to determine their stability[64,65]:

$$\Delta E = \frac{E_{\text{total}} - \sum nE_a}{N}, \tag{4}$$

where E_a is the ground state energy of a single atom, n is the number of atoms of that species, and N represents the total number of atoms in a unit cell. The energy of a single atom can be calculated by optimizing an isolated atom. The calculated formation energies of Cs_2InBiF_6, $Cs_2InBiCl_6$, $Cs_2InBiBr_6$, and Cs_2InBiI_6 are −3.54 eV, −5.46 eV, −10.06 eV, and −15.12 eV, respectively. The negative formation energies confirm the thermodynamic stability of these compounds.

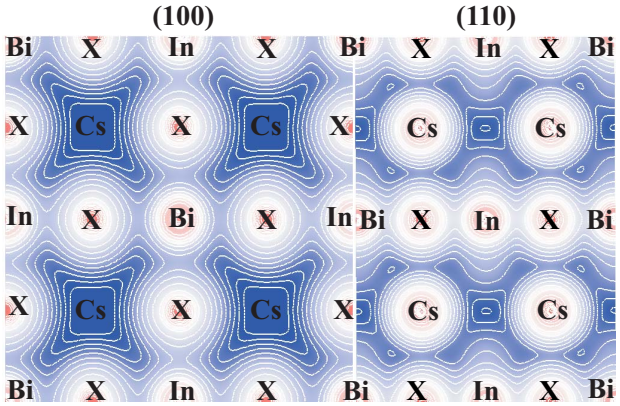

Fig. 3. Electronic charge density contours in the [100,110] planes.

3.2. Chemical Bonding

For studying bonding aspects of these materials, we examine the electron charge densities of the understudy compounds. The electron charge densities for crystal planes (100) and (110) are plotted in Fig. 3. The overlapping counters between Bi and X atoms in the (100) plane reveal a covalent bond and correspond to BiX_6 octahedra. In plane (110), the counters In and X overlap each other, which confirm covalent bonds and correspond to InX_6 octahedra. The non-overlapping and spherical symmetric counters of Cs show ionic bonds between Cs and X. The calculated bond lengths are listed in Table 1. The table reveals that the bond lengths increase from Cl to I, and this increase is related to the decreasing electronegativity and increasing size of the halogens. The electronegativities of Cs, In, Bi, F, Cl, Br, and I are 0.79, 1.78, 2.02, 3.98, 3.16, 2.96, and 2.66, respectively, on a puling scale basis.

3.3. Electronic Properties

In order to examine the electronic nature, the band structure and density of states (DOS) are used to look at whether materials are insulators, conductors, or semiconductors. The band structure and DOS calculations are performed using GGA, mBJ, and mBJ + SOC. Figure 4 reveals that Cs_2InBiX_6 (X = F, Cl, Br, I) is direct band gap materials. The valence band maximum (VBM) and conduction band minimum (CBM) both lie on the same Γ symmetry line of the Brillouin zone. Direct band gap materials are more efficient for optoelectronic applications as compared to indirect band gap because of phonon involvement, which make indirect band gap semiconductors bad emitters of light[57,58]. Zhao *et al.*[49] and Xiao *et al.*[53] also reported direct band gaps of Cs_2InBiX_6 (X = F, Cl, Br, I) using the HSE + SOC method. Figure 4 shows that SOC pushed the valence and conduction bands toward the Fermi level that caused reduction of the band gaps in these compounds. SOC splits the Bi 6p in the conduction band, pushing one of the orbitals toward the Fermi level and reducing the band gap. The band gap values are listed in Table 1. GGA underestimates band gaps of Cs_2InBiX_6 (X = F, Cl, Br, I). Our results calculated with mBJ + SOC are consistent

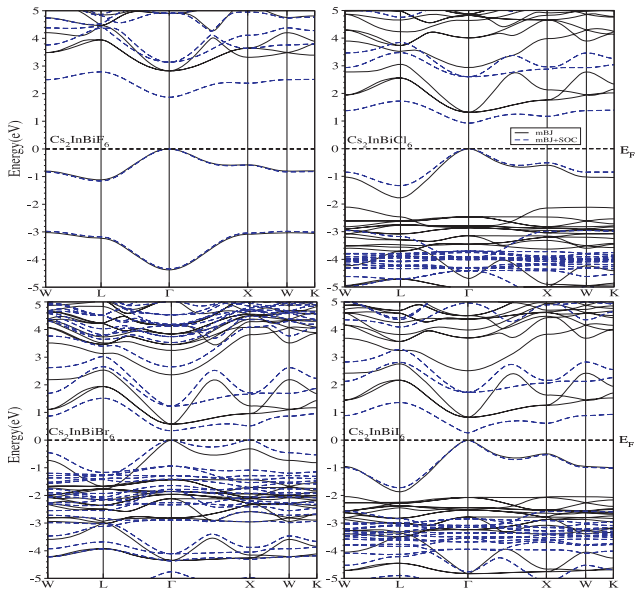

Fig. 4. Electronic band structures of Cs_2InBiX_6 (X = F, Cl, Br, I).

with the reported data[49,53]. MBJ is renowned for its excellent band gap production near the experimental values. The calculated band gap value of $Cs_2InBiCl_6$ is closer (the best solar cell material $MAPbI_3$ has a band gap of 1.55 eV) to the optimal value for photovoltaic performance (1.4 eV)[66].

DOS is mostly used for physical properties of materials like dielectric spectra, photoemission spectra, and transport properties. It shows the role and location of different energy orbitals in the formation of a band structure. Total DOS and partial DOS of Cs_2InBiF_6, $Cs_2InBiCl_6$, $Cs_2InBiBr_6$, and Cs_2InBiI_6 compounds are given in Figs. 5 and 6, respectively. The Fermi level separates the valence and conduction bands. From the total DOS, it is clear

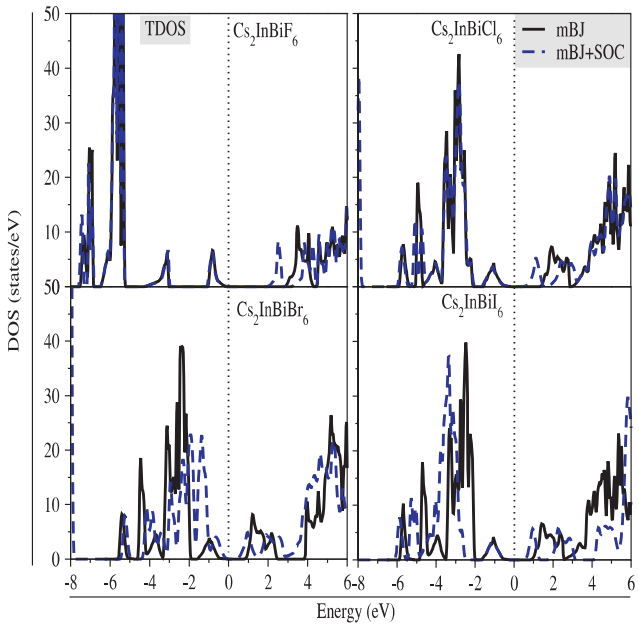

Fig. 5. Total density of states of Cs_2InBiX_6 (X = F, Cl, Br, I).

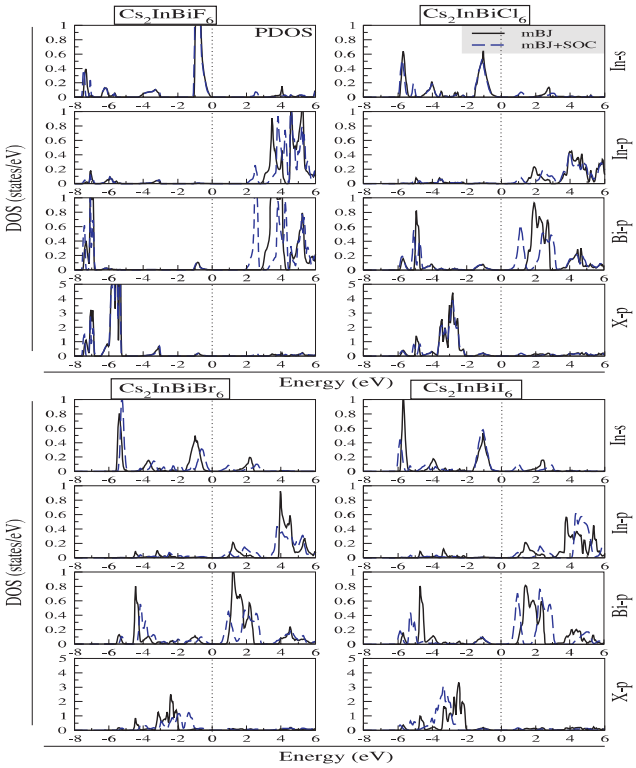

Fig. 6. Partial density of states of Cs_2InBiX_6 (X = F, Cl, Br, I).

that SOC pushes the conduction band towards the Fermi level, which reduces band gaps of these metal halides. The partial DOS demonstrates that In 5s contributes to VBM. The halogen p orbitals have a dominant role in the formation of bands in the energy range of −2 to −4 eV in the valence band. Bi 6p orbitals have contributed bands at energy of −4.5 eV in the valence band.

The CBM is derived primarily from the Bi 6p orbitals, whereas In 5p orbitals have significant contributions in the energy range from 4 to 6 eV in the conduction band. The small band gaps of Cs_2InBiX_6 compared to other metal halide perovskites are due to the fact that strong sp coupling between the 5s state of In and p orbitals of halogen endorses the VBM to relatively high energy with respect to the CBM[67]. Figure 6 also reveals that SOC splits Bi 6p orbitals in the conduction bands and pushes one of the Bi 6p orbitals towards the Fermi level, which further reduces the band gap of these compounds. The high energy In $5s^2$ states, which occupy VBM, are mainly responsible for the promising photovoltaic properties of Cs_2InBiX_6 (X = Cl, Br, I)[53]. Such high energy states at the top of the valence band are stable with respect to decomposition[49].

Band dispersion and carrier effective masses play a vital role in the efficiency of solar cells and other optoelectronic materials. The VBM and the CBM of Cs_2InBiX_6 (X = F, Cl, Br, I) are located at Γ symmetry of the Brillouin zone and have large band dispersion. This large band dispersion results in the small carrier effective masses[49]. The effective masses of electrons and holes are calculated from the parabolic fitting of the band edges according to the relation

$$m^* = \hbar^2 \left[\frac{\partial^2 \varepsilon(k)}{\partial k^2} \right]^{-1}, \tag{5}$$

where $\varepsilon(k)$ and k represent band edge eigen values and wave vectors, respectively. The effective masses of electrons (m_e^*) and holes (m_h^*) are listed and compared with the reported data in Table 1. The table reveals that Cs_2InBiX_6 has quit small carrier effective masses. Our calculated values of the carrier effective masses are in good agreement with the reported work[48]. The effective masses are also compared with $MAPbI_3$. It is evident from the table that SOC not only splits the band but also alters the values of the carrier effective masses.

3.4. Optical Properties

The interaction of light with the material medium is expressed in terms of optical properties. Presently, we study optical properties of metal halide double perovskites Cs_2InBiX_6 (X = F, Cl, Br, I) under the DFT scheme by measuring their different optical parameters.

The study of polarization and absorption of electromagnetic radiation within the material medium is expressed in dielectric functions, which are mathematically presented by a relation $\varepsilon(\omega) = \varepsilon_1(\omega) + i\varepsilon_2(\omega)$. In this relation, the first term represents the real part $\varepsilon_1(\omega)$, which shows polarization of light, while the second term represents imaginary part $\varepsilon_2(\omega)$ of the dielectric function, which measures the extent of light absorption. The calculated zero frequency limits (static dielectric constant) $\varepsilon_1(0)$ are listed and compared in Table 2. This reveals that $\varepsilon_1(0)$ increases as the band gap decreases from F to I, meaning that band gap energy has an inverse relation to $\varepsilon_1(0)$, which is consistent with the Penn model[68]. These compounds have remarkable large values of $\varepsilon_1(0)$ comparable with that of $MAPbI_3$ and $CsPbI_3$. The maximum value of $\varepsilon_1(\omega)$ is observed in the visible energy range (2–2.5 eV) and then rapidly decreases, and small humps are observed, which can be related to interband transitions between valence and conduction bands. $MAPbI_3$ has a dielectric constant of 6.5 in the visible spectral range at the temperature of 4.2 K[71]. The understudy compounds have larger values of dielectric function than $MAPbI_3$ in the visible spectral region.

The imaginary part of the dielectric function is the measure of the extent of light absorption. It is a seed parameter and can be directly calculated from the Fermi–Golden rule; all other optical parameters including $\varepsilon_1(\omega)$ are calculated from $\varepsilon_2(\omega)$. The first onsets of absorption (absorption edge) are observed roughly at 2.75, 1.35, 0.80, and 0.80 eV for Cs_2InBiF_6, $Cs_2InBiCl_6$, $Cs_2InBiBr_6$, and Cs_2InBiI_6, respectively. These onsets are close to the fundamental band gaps of these compounds. The absorption edge of $Cs_2InBiCl_6$ is very close to that of $MAPbI_3$, which is found at ~1.55 eV[71]. Halogen substitution significantly changes the positional occurrence of the transition peaks. High absorption peaks are observed in the visible spectral region at energy around 2–3 eV. Several weak peaks are observed in the energy range of 3–15 eV.

Knowledge of the refractive index $n(\omega)$ is necessary for the effective use of a material in photonic and optical devices. Refractive indices are inversely proportional to the band gap of a material, i.e., wide band gap materials have small values of refractive indices and vice versa. The refractive indices for Cs_2InBiX_6 (X = F, Cl, Br, I) compounds are shown in Fig. 7. The zero frequency limit of refractive index $n(0)$ values are listed in Table 2. The maximum peaks of the index of refraction for $Cs_2InBiCl_6$, $Cs_2InBiBr_6$, and Cs_2InBiI_6 are observed in the energy range of 2–2.5 eV for these compounds. The peak values are larger than the refractive index of $MAPbI_3$ (2.61) in the

Table 2. The Zero-Frequency Values of the Real Part of the Dielectric Function and Refractive Index.

Compounds	$\varepsilon_1(0)$	$n(0)$
Cs_2InBiF_6	2.73	1.66
$Cs_2InBiCl_6$	4.65	2.10
$Cs_2InBiBr_6$	6.00	2.47
Cs_2InBiI_6	6.10	2.49
$CsPbI_3$	5.00[a]	2.1[a]
$MAPbI_3$	6.00[b]	1.68[b]

[a]Reference [69].

[b]Reference [70].

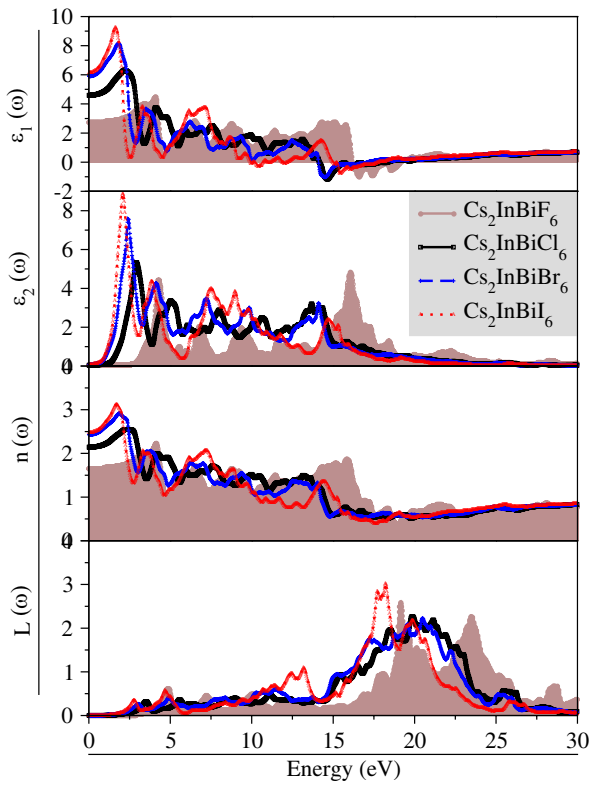

Fig. 7. Frequency dependent optical parameters of Cs_2InBiX_6 (X = F, Cl, Br, I).

visible spectral range[71]. Appreciable values of $n(\omega)$ below 4.5 eV suggest that Cs_2InBiX_6 is opaque against light. It explores interactions of the incident photons and explains various features of a semiconductor. The calculated $L(\omega)$ for Cs_2InBiX_6 is plotted in Fig. 7, in which no scattering happens when the energy of the photon is less than the band gap energy. The highest peaks appear at the energy range of 17–20 eV. These peaks show plasma resonance, and their frequencies are called plasma frequencies.

3.5. Mechanical Properties

The mechanical properties of a material play an important role in structure stability and strength of a material to an exterior force, and are associated with basic phenomena of solid state, like inter-atomic bonding, phonon spectra, and equation of state. Mechanical properties are computed using independent elastic coefficients C_{ij} calculated using the Charpin package embedded in Wien2k and listed in Table 3.

The calculated results satisfy the Born mechanical stability criteria, i.e., $C_{11} + 2C_{12} > 0, C_{44} > 0, \quad C_{11} - C_{12} > 0,$ and $C_{12} < C_{11}$[72], which show that these compounds are a mechanically stable perovskite structure. Resistance of a material to reversible deformation upon shear stress is calculated from shear modulus (G), which gives information about the rigidity of a material; thus, G is calculated using two models Voigt (G_V)[73] and Reuss (G_R)[74]:

$$G_V = \frac{1}{5}(3C_{44} + C_{11} - C_{12}), \tag{6}$$

$$G_R = \frac{5(C_{11} - C_{12})C_{44}}{4C_{44} + 3(C_{11} - C_{12})}. \tag{7}$$

However, Hill[75] (G_H) calculated the arithmetic mean of G_V and G_R:

$$G_H = \frac{G_V + G_R}{2}. \tag{8}$$

The calculated values of G_H show that Cs_2InBiI_6 has the highest value (43.3 GPa) of shear modulus, which clarifies that it is stiffer than the rest of the materials. The reaction of a material to linear deformation can be determined from Young's modulus (Y), i.e., the toughness of a material depends on the value of Y. The higher the value of Y, the greater the toughness of a material will be, which is calculated using the relation

$$Y = \frac{9BG_V}{3B + G_V}. \tag{9}$$

The larger value of Y (103.2 GPa) for Cs_2InBiF_6 indicates a high toughness among these compounds. Pugh's ratio (B/G) can be used to examine the ductile/brittle nature of a material[76]; material is ductile if the value of B/G is less than 1.75, otherwise it represents a brittle nature. Pettifog and Chen have established the brittle versus ductile transition in different materials using first principles calculations[77,78]. Our calculated results show that these compounds have lesser value of B/G than the critical value of 1.75, which confirm that these materials are brittle in nature. The bonding nature of a material can be explained with the help of Cauchy pressure[78]. The value of Cauchy pressure is determined using the following equation:

$$C'' = C_{12} - C_{44}. \tag{10}$$

Lower values of Cauchy pressure show directional response in bonding (covalent bonding), while higher values of Cauchy pressure result in ionic bonding. The values of C'' mentioned in Table 3 confirm that these compounds are brittle in nature. The compressibility is measured with the help of Poisson's ratio ν, which is the ratio of adjacent longitudinal strain in non-axial tensile stress:

$$\nu = \frac{3B - Y}{6B}. \tag{11}$$

A material having $\nu < 0.5$ is considered incompressible[79], and $\nu \geq 0.5$ has the tendency of compressibility, i.e., stretching a sample causes no adjacent reduction, so its volume remains the same no matter how distorted it is. The values of Poisson's ratio for compounds Cs_2InBiX_6 (X = F, Cl, Br, I) lie in the range of 0.05–0.21, which show that these materials are incompressible.

Table 3. Calculated Values of Elastic Constants C_{ij}, Shear Modulus G, Young's Modulus Y, Bulk Modulus B, Shear Constant C', Cauchy Pressure C'', B/G Ratio, ν, ζ, A, λ, and μ Parameters.

Parameters	X = F	X = Cl	X = Br	X = I
C_{11} (GPa)	98	81	105	71
C_{12} (GPa)	35	28	31	20
C_{44} (GPa)	57	44	41	62
G_V (GPa)	46.8	37.0	39.4	47.4
G_R (GPa)	43.0	34.8	39.3	39.4
G_H (GPa)	44.9	35.9	39.3	43.4
Y (GPa)	103.2	87.3	95.6	99.6
B (GPa)	49.2	45.6	55.6	37.0
B/G	1.09	1.27	1.41	0.85
C''	−22	−16	−10	−42
ν	0.15	0.18	0.21	0.05
Z	0.61	0.59	0.52	0.50
A	1.80	1.66	1.100	2.43
C'	31.5	26.5	37.00	25.5
λ	19.1	21	29.4	5.4
μ	60.7	37	39.4	47.4

The anisotropic parameter (A) of a material is given as

$$A = \frac{2C_{44}}{C_{11} - C_{12}}. \tag{12}$$

For an ideal isotropic system, the value of A is unity and diverges from unity for anisotropic systems. The calculated values are 1.80, 1.66, 1.100, and 2.43 for Cs_2InBiF_6, $Cs_2InBiCl_6$, $Cs_2InBiBr_6$, and Cs_2InBiI_6, respectively, which show the anisotropic nature of these materials. Shear constant (C') is another significant parameter, which explains the stability of a material:

$$C' = \frac{1}{2}(C_{11} - C_{12}). \tag{13}$$

The stability of a material requires $C' > 0$, so the calculated positive values of C show that these compounds are elastically stable. The interior straining of a compound can be examined by a parameter called the Kleinman parameter (ζ)[80]. It explains the bond stretching versus bond bending given as

$$\xi = \frac{C_{11} + 8C_{12}}{7C_{11} - 2C_{12}}. \tag{14}$$

The zero value of ζ indicates minimization of bond bending, while $\zeta = 1$ indicates minimization of bond stretching. The tabulated values confirm bond stretching in these compounds. Another motivating mechanical parameter is Lame's constants (λ, μ), which are used to define anisotropy of a material:

$$\lambda = \frac{Y\nu}{(1+\nu)(1-2\nu)}, \tag{15}$$

$$\mu = \frac{Y}{2(1-\nu)}. \tag{16}$$

For isotropic materials, $\lambda = C_{12}$ and $\mu = C'$. The calculated Lame's coefficients of Cs_2InBiX_6 (X = F, Cl, Br, I) are given in Table 3, confirming the results obtained from the anisotropic parameter (A) and showing that these materials are anisotropic.

4. Conclusions

It is summarized that the understudy compounds Cs_2InBiX_6 (X = F, Cl, Br and I) are theoretically investigated in the framework of the DFT. Goldschmidt's tolerance factor, octahedral factor, the newly proposed tolerance factor, formation energy, and elastic constant demonstrate that these compounds possess a stable perovskite structure. The mechanical parameters reveal that these compounds are brittle and anisotropic. These perovskites are optically active materials in the infrared spectral region. The substitution of the anion tuned the band gap from 2.79 to 0.80 eV. The valence band is dominated by In s and X p orbitals, where the conduction band is mostly made of Bi p states. High dielectric materials comparable to $MAPbI_3$ are found, and interesting variations are observed in their optical properties.

References

1. J. Tong, Z. Song, D. H. Kim, X. Chen, C. Chen, A. F. Palmstrom, P. F. Ndione, M. O. Reese, S. P. Dunfield, O. G. Reid, J. Liu, F. Zhang, S. P. Harvey, Z. Li, S. T. Christensen, G. Teeter, D. Zhao, M. M. Al-Jassim, M. F. A. M. van Hest, M. C. Beard, S. E. Shaheen, J. J. Berry, Y. Yan, and K. Zhu, "Carrier lifetimes of > 1 μs in Sn-Pb perovskites enable efficient all-perovskite tandem solar cells," Science **364**, 475 (2019).
2. P. R. Varadwaj, "$A_2AgCrCl_6$ (A = Li, Na, K, Rb, Cs) halide double perovskites: a transition metal-based semiconducting material series with appreciable optical characteristics," Phys. Chem. Chem. Phys. **22**, 24337 (2020).
3. M. Ghasemi, M. Hao, M. Xiao, P. Chen, D. He, Y. Zhang, W. Chen, J. Fan, J. H. Yun, B. Jia, and X. Wen, "Lead-free metal-halide double perovskites: from optoelectronic properties to applications," Nanophotonics, https://doi.org/10.1515/nanoph-2020-0548 (2020).
4. Y. Fu, H. Zhu, J. Chen, M. P. Hautzinger, X. Y. Zhu, and S. Jin, "Metal halide perovskite nanostructures for optoelectronic applications and the study of physical properties," Nat. Rev. Mater. **4**, 169 (2019).
5. Q. Jiang, Y. Zhao, X. Zhang, X. Yang, Y. Chen, Z. Chu, Q. Ye, X. Li, Z. Yin, and J. You, "Surface passivation of perovskite film for efficient solar cells," Nat. Photon. **13**, 460 (2019).
6. N. J. H. Lm, S. H. Heo, J. H. Mandal, and T. N. S. I. Seok, "Chemical management for colorful, efficient and stable inorganic–organic hybrid nanostructured solar cells," Nano Lett. **13**, 1764 (2013).
7. S. D. Stranks, G. E. Eperon, G. Grancini, C. Menelaou, M. J. Alcocer, T. Leijtens, and H. J. Snaith, "Electron-hole diffusion lengths exceeding 1 micrometer in an organometallic trihalide perovskite absorber," Science **342**, 341 (2013).
8. Q. Dong, Y. Fang, Y. Shao, P. Mulligan, J. Qiu, L. Cao, and J. Huang, "Electron-hole diffusion lengths >175 μm in solution-grown $CH_3NH_3PbI_3$ single crystals," Science, **347**, 967 (2015).
9. D. Shi, V. Adinolfi, R. Comin, M. Yuan, E. Alarousu, A. Buin, Y. Chen, S. Hoogland, A. Rothenberger, K. Katsiev, Y. Losovyj, X. Zhang, P. A. Dowben, O. F. Mohammed, E. H. Sargent, and O. M. Bakr, "Low trap-state density and long carrier diffusion in organo lead trihalide perovskite single crystals," Science **347**, 519 (2015).
10. M. A. Green, A. Ho-Baillie, and H. J. Snaith, "The emergence of perovskite solar cells," Nat. Photon. **8**, 506 (2014).
11. J. Suntivich, H. A. Gasteiger, N. Yabuuchi, H. G. Nakanishi, J. B. Enough, and S. Horn, "Design principles for oxygen-reduction activity on perovskite oxide catalysts for fuel cells and metal–air batteries," Nat. Chem. **3**, 546 (2011).
12. N. Wang, L. Cheng, R. Ge, S. Zhang, Y. Miao, W. Zou, and Y. Wei, "Perovskite light-emitting diodes based on solution-processed self-organized multiple quantum wells," Nat. Photon. **10**, 699 (2016).
13. S. Park, W. J. Chang, C. W. Lee, S. Park, H. Y. Ahn, and K. T. Nam, "Photocatalytic hydrogen generation from hydriodic acid using methylammonium lead iodide in dynamic equilibrium with aqueous solution," Nat. Energy **2**, 16185 (2017).
14. L. Bellaiche and D. Vanderbilt, "Virtual crystal approximation revisited: application to dielectric and piezoelectric properties of perovskites," Phys. Rev. B **61**, 7877 (2000).
15. Q. Chen, J. Wu, X. Ou, B. Huang, J. Almutlaq, A. A Zhumekenov, X. Guan, S. Han, L. Liang, Z. Yi, J. Li, X. Xie, Y. Wang, Y. Li, D. Fan, D. B. L. Teh, A. H. All, O. F. Mohammed, O. M. Bakr, T. Wu, M. Bettinelli, H. Yang, W. Huang, and X. Liu, "All-inorganic perovskite nanocrystal scintillators," Nature **561**, 88 (2018).
16. H. Zhu, Y. Fu, F. Meng, X. Wu, Z. Gong, Q. Ding, M. V. Gustafsson, M. T. Trinh, S. Jin, and X.-Y. Zhu, "Lead halide perovskite nanowire lasers with low lasing thresholds and high quality factors," Nat. Mater. **14**, 636 (2015).
17. A. Kostopoulou, K. Brintakis, N. K. Nasikas, and E. Stratakis, "Perovskite nanocrystals for energy conversion and storage," Nanophotonics **8**, 1607 (2019).
18. J. Zhou, Z. Xia, M. S. Molokeev, X. Zhang, D. Peng, and Q. Liu, "Composition design, optical gap and stability investigation of lead-free halide double perovskite $Cs_2AgInCl_6$," J. Mater Chem. A **5**, 15031 (2017).
19. N. K. Noel, S. D. Stranks, A. Abate, C. Wehrenfennig, S. Guarnera, A. A. Haghighirad, A. Sadhanala, G. E. Eperon, S. K. Pathak, M. B. Johnston, A. Petrozza, L. M. Herz, and H. J. Snaith, "Lead free organic

and inorganic tin halide perovskites for photovoltaic applications," Energy Environ. Sci. **7**, 3061 (2014).
20. Y. Fang, Q. Dong, Y. Shao, Y. Yuan, and J. Huang, "Highly narrowband perovskite single crystal photo detectors enabled by surface-charge recombination," Nat. Photon. **9**, 679 (2015).
21. A. Kojima, K. Teshima, Y. Shirai, and T. Miyasaka, "Organometal halide perovskites as visible-light sensitizers for photovoltaic cells," J. Am. Chem. Soc. **131**, 6050 (2009).
22. M. M. Lee, J. Teuscher, T. Miyasaka, T. N. Murakami, and H. J. Snaith, "Efficient hybrid solar cells based on meso-superstructured organometal halide perovskites," Science **338**, 643 (2012).
23. H. S. Kim, C. R. Lee, J. H. Im, K. B. Lee, T. Moehl, A. Marchioro, S. J. Moon, R. Humphry-Baker, J. H. Yum, J. E. Moser, M. Grätzel, and N. G. Park, "Lead iodide perovskite sensitized all-solid-state submicron thin film mesoscopic solar cell with efficiency exceeding 9%," Sci. Rep. **2**, 591 (2012).
24. A. A Emery, J. E. Saal, S. Kirklin, V. I. Hegde, and C. Wolverton "High-throughput computational screening of perovskites for thermochemical water splitting applications," Chem. Mater. **28**, 5621 (2016).
25. J. Burschka, N. Pellet, S.-J. Moon, R. H. Baker, P. Gao, M. K. Nazeeruddin, and M. Gratzel, "Sequential deposition as a route to high-performance perovskite-sensitized solar cells," Nature **499**, 316 (2013).
26. L. Lu, X. Pan, J. Luo, and Z. Sun, "Recent advances and optoelectronic applications of lead-free halide double perovskites," Chem. Eur. J. **26**, 16975 (2020).
27. C. C. Stoumpos, L. Frazer, D. J. Clark, Y. S. Kim, S. H. Rhim, A. J. Freeman, and M. G. Kanatzidis, "Hybrid germanium iodide perovskite semiconductors: active lone pairs, structural distortions and indirect energy gaps and strong nonlinear optical properties," J. Am. Chem. Soc. **137**, 6804 (2015).
28. T. Umebayashi, K. Asai, T. Kondo, and A. Nakao, "Electronic structures of lead iodide based low-dimensional crystals," Phys. Rev. B **67**, 155405 (2003).
29. R. J. Sutton, G. E. Eperon, L. Miranda, E. S. Parrott, B. A. Kamino, J. B. Patel, and H. J. Snaith, "Bandgap -tunable cesium lead halide perovskites with high thermal stability for efficient solar cells," Adv. Enr. Mater. **6**, 1502458 (2016).
30. M. Kulbak, D. Cahen, and Hodes, "How important is the organic part of lead halide perovskite photovoltaic cells, efficient $CsPbBr_3$ cells," J. Phys. Chem. Lett. **6**, 2452 (2015).
31. X.-G. Zhao, J.-H. Yang, Y. Fu, D. Yang, Q. Xu, L. Yu, S.-H. Wei, and L. Zhang, "Design of lead-free inorganic halide perovskites for solar cells via cation-transmutation," J. Am. Chem. Soc. **139**, 2630 (2017).
32. C. J. Bartel, J. M. Clary, C. Sutton, D. Vigil-Fowler, B. R. Goldsmith, A. M. Holder, and C. B. Musgrave, "Inorganic halide double perovskites with optoelectronic properties modulated by sublattice mixing," J. Am. Chem. Soc. **142**, 5135 (2020).
33. J. D. Majher, M. B. Gray, T. A. Strom, and P. M. Woodward, "$Cs_2NaBiCl_6$: Mn^{2+}–a new orange-red halide double perovskite phosphor," Chem. Mater. **31**, 1738 (2019).
34. S. Vasala and M. Karppinen, "$A_2B'B''O_6$ perovskites," Rev. Pro. Sol. Stat. Chem. **43**, 1 (2015).
35. R. F. Berger and J. B. Neaton, "Computational design of low-band-gap double perovskites," Phys. Rev. B **86**, 165211 (2012).
36. L. R. Morss, M. Siegal, L. Stenger, and N. Edelstein, "Preparation of cubic chloro complex compounds of trivalent metals: Cs_2NaMCl_6," Inorg. Chem. **9**, 1771 (1970).
37. W. M. A. Smit, G. J. Dirksen, and D. J. Stufkens, "Infrared and Raman spectra of the elpasolites $Cs_2NaSbCl_6$ and $Cs_2NaBiCl_6$: evidence for a pseudo Jahn–Teller distorted ground state," J. Phys. Chem. Solid **51**, 189 (1990).
38. P. Barbier, M. Drache, G. Mairesse, and J. Ravez, "Phase transitions in a $Cs_{2-x}K_{1+x}BiCl_6$ solid solution," J. Sol. State Chem. **42**, 130 (1982).
39. F. Benachenhou, G. Mairesse, G. Nowogrocki, and D. Thomas, "Structural studies of Cs-K-Bi mixed chlorides relation to the crystal structures of A_2BMX_6, A_3MX_6, and A_2MX_6," J. Sol. State Chem. **65**, 13 (1986).
40. D. P. McMeekin, G. Sadoughi, W. Rehman, G. E. Eperon, M. Saliba, M. T. Hörantner, A. Haghighirad, M. B. Johnston, N. Sakai, L. Korte, B. Rech, M. B. Johnston, L. M. Herz, and H. J. Snaith, "A mixed-cation lead mixed-halide perovskite absorber for tandem solar cells," Science **351**, 151 (2016).
41. H. Choi, J. Jeong, H. B. Kim, S. Kim, B. Walker, G. H. Kim, and J. Y. Kim, "Cesium-doped methyl ammonium lead iodide perovskites light absorber for hybrid solar cells," Nano. Energy **7**, 80 (2014).
42. C. Yi, J. Luo, S. Meloni, A. Boziki, N. Ashari-Astani, C. Grätzel, and M. Grätzel, "Entropic stabilization of mixed A-cation ABX_3 metal halide perovskites for high performance perovskite solar cells," Energy. Environ. Sci. **9**, 656 (2016).
43. Z. Li, M. Yang, J. S. Park, S. H. Wei, J. J. Berry, and K. Zhu, "Stabilizing perovskite structures by tuning tolerance factor: formation of formamidinium and cesium lead iodide solid-state alloys," Chem. Mater. **28**, 284 (2015).
44. W. Urland, "The assessment of the crystal field parameters for f^n-electron systems by the angular overlap model. Rare-earth ions M^{3+} in $C_{s2}NaMCl_6$," Chem. Phys. Lett. **83**,116 (1981).
45. A. H. Slavney, T. Hu, A. M. Lindenberg, H. I. Karunadasa, and A. B. Halde, "Double perovskite with long carrier recombination lifetime for photovoltaic applications," J. Am. Chem. Soc. **138**, 2138 (2016).
46. E. T. McClure, M. R. Ball, W. Windl, and P. M. Woodward, "Cs_2AgBiX_6 (X = Br, Cl): new visible light absorbing, lead-free halide perovskites semiconductors," Chem. Mater. **28**, 1348 (2016).
47. G. Volonakis, A. A. Haghighirad, H. J. Snaith, and F. Giustino, "Route to stable lead-free double perovskites with the electronic structure of $CH_3NH_3PbI_3$: a case for mixed-cation $[Cs/CH_3NH_3/CH(NH_2)_2]_2InBiBr_6$," J. Phys. Chem. Lett. **8**, 3917 (2017).
48. G. Volonakis, M. R. Filip, A. A. Haghighirad, N. Sakai, B. Wenger, and H. J. Snaith, "Lead-free halide double perovskites via heterovalent substitution of noble metals," J. Phys. Chem. Lett. **7**, 1254 (2016).
49. F. Bachhuber, J. von Appen, R. Dronskowski, P. S. Nilges, T. A. Pfitzner, and R. Weihrich, "The extended stability ranges of phosphorus allotropes," Ang. Chemie. Interna. Edit. **53**, 11629 (2014).
50. G. Volonakis, A. A. Haghighirad, R. L. Milot, W. H. Sio, M. R. Filip, B. Wenger, and F. Giustino "$Cs_2InAgCl_6$: a new lead-free halide double perovskite with direct band gap," J. Phys. Chem. Lett. **8**, 772 (2017).
51. F. Wei, Z. Deng, S. Sun, T. Xie, G. Kieslich, D. M. Evans, and A. K. Cheetham, "The synthesis structure and electronic properties of a lead-free hybrid inorganic–organic double perovskite $(MA)_2KBiCl_6$ (MA= methylammonium)," Mater. Horizo. **3**, 328 (2016).
52. Z. Deng, F. Wei, S. Sun, G. Kieslich, A. K. Cheetham, and P. D. Bristowe, "Exploring the properties of lead-free hybrid double perovskites using a combined computational experimental approach," J. Mater. Chem. A **4**, 12025 (2016).
53. Z. Xiao, K. Z. Du, W. Meng, J. Wang, D. B. Mitzi, and Y. Yan, "Intrinsic instability of $Cs_2In(I)M(III)X_6$ (M = Bi, Sb; X = halogen) double perovskites: a combined density functional theory and experimental study," J. Am. Chem. Soc. **139**, 6054 (2017).
54. P. Blaha, K. Schwarz, F. Tran, R. Laskowski, G. K. H. Madsen, and L. D. Marks, "WIEN2k: an APW+lo program for calculating the properties of solids," J. Chem. Phys. **152**, 074101 (2020).
55. J. P. Perdew, A. Ruzsinszky, G. I. Csonka, O. A. Vydrov, G. E. Scuseria, L. A. Constantin, X. Zhou, and K. Burke, "Restoring the density-gradient expansion for exchange in solids and surfaces," Phys. Rev. Lett. **100**, 136406 (2008).
56. H. Jiang, "Structural and electronic properties of ZrX_2 and HfX_2 (X = S and Se) from first principles calculations," J. Chem. Phys. **134**, 204705 (2011).
57. I. Khan, I. Ahmad, H. A. R. Aliabad, and M. Maqbool, "Effect of phase transition on the optoelectronic properties of $Zn_{1-x}Mg_xS$," J. Appl. Phys. **112**, 073104 (2012).
58. I. Khan, I. Ahmad, H. A. R. Aliabad, S. J. Asadabadi, Z. Ali, and M. Maqbool, "Conversion of optically isotropic to anisotropic CdS_xSe_{1-x} ($0 \le x \le 1$) alloy with S concentration," Comp. Mater. Sci. **77**, 145 (2013).
59. F. Tran and P. Blaha, "Accurate band gaps of semiconductors and insulators with a semilocal exchange-correlation potential," Phys. Rev. Lett. **102**, 226401 (2009).
60. B. Traoré, G. Bouder, W. L. D. Hauret, X. Rocquefelte, C. Katan, F. Tran, and M. Kepenekian, "Efficient and accurate calculation of band gaps of halide perovskites with the Tran–Blaha modified Becke–Johnson potential," Phys. Rev. B **99**, 035139 (2019).
61. F. Birch, "Finite elastic strain of cubic crystals," Phys. Rev. **71**, 809 (1947).
62. P. Umari, E. Mosconi, and F. De Angelis, "Relativistic GW calculations on $CH_3NH_3PbI_3$ and $CH_3NH_3SnI_3$ perovskites for solar cell applications," Sci. Rep. **4**, 4467 (2014).
63. F. Igbari, Z. K. Wang, and L. S. Liao, "Progress of lead-free halide double perovskites," Adv. Energy Mater. **9**, 1803150 (2019).

64. M. Pozzo and D. Alfè, "Structural properties and enthalpy of formation of magnesium hydride from quantum Monte Carlo calculations," Phys. Rev. B **77**, 104103 (2008).
65. H. Zhang, S. Shang, J. E. Saal, A. Saengdeejing, Y. Wang, L. Q. Chen, and Z. K. Liu, "Enthalpies of formation of magnesium compounds from first-principles calculations," Intermetallics **17**, 878 (2009).
66. M. K. Assadi, S. Bakhoda, R. Saidur, and H. Hanaei, "Recent progress in perovskite solar cells," Renew. Sust. Energy Rev. **81**, 2812 (2018).
67. P. Zhang, J. Yang, and S. H. Wei, "Manipulation of cation combinations and configurations of halide double perovskites for solar cell absorbers," J. Mater. Chem. A **6**, 1809 (2018).
68. D. Penn, "Wave-number-dependent dielectric function of semiconductors," Phys. Rev. **128**, 2093 (1962).
69. M. Ahmad, G. Rehman, L. Ali, M. Shafiq, R. Iqbal, R. Ahmad, T. Khan, S. J. Asadabadi, M. Maqbool, and I. Ahmad, "Structural, electronic and optical properties of $CsPbX_3$ (X = Cl, Br, I) for energy storage and hybrid solar cell applications," J. Alloys Compd. **705**, 828 (2017).
70. J. Ma and L. W. Wang, "Nanoscale charge localization induced by random orientations of organic molecules in hybrid perovskite $CH_3NH_3PbI_3$," Nano Lett. **15**, 248 (2015).
71. P. Loöper, M. Stuckelberger, B. Niesen, J. Werner, M. Filipic, S. J. Moon, J. H. Yum, M. Topic, S. D. Wolf, and C. Ballif, "Complex refractive index spectra of $CH_3NH_3PbI_3$ perovskite thin films determined by spectroscopic ellipsometry and spectrophotometry," J. Phys. Chem. Lett. **6**, 66 (2015).
72. M. Born, *On the Stability of Crystal Lattices* (Cambridge University, 1940).
73. W. Voigt, *Lehrbuch der Kristallphysik*, 2nd ed. (Taubner, 1928).
74. A. Reuss and Z. Angew, "Berechnung der Fließgrenze von Mischkristallen auf Grund der Plastizitätsbedingung für Einkristalle," Math. Mech. **9**, 49 (1929).
75. R. Hill, "The elastic behaviour of a crystalline aggregate," Proc. Phys. Soc. **65**, 349 (1952).
76. M. Orio, D. A. Pantazis, and F. Neese, "Density functional theory," Photosynth. Res. **102**, 443 (2009).
77. D. G. Pettifor, "Theoretical predictions of structure and related properties of intermetallic," Mater. Sci. Technol. **8**, 345 (1992).
78. K. Chen, L. R. Zhao, J. Rodgers, and J. S. Tse, "Alloying effects on elastic properties of tin-based nitrides," Phys. D. Appl. Phys. **36**, 2725 (2003).
79. P. H. Mott, J. R. Dorgan, and C. M. Roland, "The bulk modulus and Poisson's ratio of incompressible materials," Sound Vib. **312**, 572 (2008).
80. L. Kleinman, "Deformation potentials in silicon uniaxial strain," Phys. Rev. **128**, 2614 (1962).